Radiomics in Vulvar Cancer: First Clinical Experience Using ^{18}F-FDG PET/CT Images

Angela Collarino[1,2], Giorgia Garganese[3], Simona M. Fragomeni[3], Lenka M. Pereira Arias-Bouda[1,4], Francesco P. Ieria[2], Ronald Boellaard[5], Vittoria Rufini[2], Lioe-Fee de Geus-Oei[1,6], Giovanni Scambia[3], Renato A. Valdés Olmos[1,7], Alessandro Giordano[2], Willem Grootjans*[1], and Floris HP van Velden*[1,8]

[1]Section of Nuclear Medicine, Department of Radiology, Leiden University Medical Center, Leiden, The Netherlands; [2]Institute of Nuclear Medicine, Fondazione Policlinico Universitario A. Gemelli–IRCCS, Rome, Italy; [3]Division of Gynecologic Oncology, Department of Woman and Child Health, Fondazione Policlinico Universitario A. Gemelli–IRCCS, Rome, Italy; [4]Department of Nuclear Medicine, Alrijne Ziekenhuis, Leiderdorp, The Netherlands; [5]Department of Radiology and Nuclear Medicine, VU University Medical Center, Amsterdam, The Netherlands; [6]Biomedical Photonic Imaging Group, MIRA Institute, University of Twente, Enschede, The Netherlands; [7]Interventional Molecular Imaging Laboratory, Department of Radiology, Leiden University Medical Center, Leiden, The Netherlands; and [8]Medical Physics, Department of Radiology, Leiden University Medical Center, Leiden, The Netherlands

This study investigated whether radiomic features derived from preoperative PET images could predict both tumor biology and prognosis in women with invasive squamous cell carcinoma of the vulva. **Methods:** Patients were retrospectively included if they had a unifocal primary cancer at least 2.6 cm in diameter, received a preoperative ^{18}F-FDG PET/CT scan followed by surgery, and had at least 6 mo of follow-up data. ^{18}F-FDG PET images were analyzed by semiautomatically drawing a volume of interest on the primary tumor in each PET image, followed by extraction of 83 radiomic features. Unique radiomic features were identified by principal-component analysis (PCA), after which they were compared with histopathology using nonpairwise group comparison and linear regression. Univariate and multivariate Cox regression analyses were used to correlate the identified features with progression-free survival (PFS) and overall survival (OS). Survival curves were estimated using the Kaplan–Meier method. **Results:** Forty women were included. PCA revealed 4 unique radiomic features, which were not associated with histopathologic characteristics such as grade, depth of invasion, lymph-vascular space invasion, and metastatic lymph nodes. No statistically significant correlation was found between the identified features and PFS. However, Moran's I, a feature that identifies global spatial autocorrelation, correlated with OS ($P = 0.03$). Multivariate Cox regression analysis showed that extracapsular invasion of the metastatic lymph nodes and Moran's I were independent prognostic factors for PFS and OS. **Conclusion:** Our data show that PCA is usable to identify specific radiomic features. Although the identified features did not correlate strongly with tumor biology, Moran's I was found to predict patient prognosis. Larger studies are required to establish the clinical relevance of the observed findings.

Key Words: vulvar cancer; radiomics; ^{18}F-FDG PET/CT; principal component analysis

J Nucl Med 2019; 60:199–206
DOI: 10.2967/jnumed.118.215889

Vulvar cancer is a rare gynecologic malignancy, with an incidence rate of 1.5–2.4 per 100,000 women per year (*1,2*).Vulvar squamous cell carcinoma (VSCC) accounts for 90% of all vulvar cancers (*3*), which occur mainly in elderly women (*4*). The pattern of dissemination of vulvar cancer is predominantly lymphogenic to the inguinofemoral lymph nodes, and distant metastases are rare (*5*). Thus, the most important prognostic factor is the presence of metastatic lymph nodes (*6*). Indeed, the 5-y overall survival (OS) varies from 94.7% in women without metastatic lymph nodes to 61% in women with lymph node metastases (*7*). Additional pathologic prognostic factors include the depth of stromal invasion and lymph-vascular space invasion (*8*).

Currently, the standard treatment for VSCC includes radical resection of the primary tumor followed by unilateral or bilateral surgical staging of the inguinofemoral lymph nodes. In particular, sentinel lymph node biopsy is the standard of care in cases of a naïve unifocal tumor with a diameter of 4 cm or less and clinically negative lymph nodes (cN0). Radical inguinofemoral lymphadenectomy is thus indicated in the remaining cases of negative lymph nodes and in all cases of metastatic lymph nodes (*8–10*), even if sentinel lymph node biopsy is now under investigation, being potentially safe also in the many cN0 cases considered unfit for minimal surgical procedures (*11*). Adjuvant radiotherapy is indicated on the basis of primary risk factors, such as resection margin status, depth of stromal invasion, and nodal involvement (*8,12*).

Recently, PET/CT imaging using the glucose analog ^{18}F-FDG has been included in the preoperative workup of vulvar cancer, mainly for staging (*8*). However, there is growing interest in radiomics, that is, high-throughput extraction of large amounts of imaging features (*13*), where several of these features, including

Received Jun. 6, 2018; revision accepted Jun. 11, 2018.
For correspondence or reprints contact: Angela Collarino, Section of Nuclear Medicine, Department of Radiology, Leiden University Medical Center, Albinusdreef 2, 2333 ZA Leiden, The Netherlands.
E-mail: angelacollarino@tiscali.it
*Contributed equally to this work.
Published online Jul. 20, 2018.

descriptors that quantify tracer uptake—morphology and tracer uptake heterogeneity—are predictive of tumor biologic behavior, response to therapy, and prognosis (*14*). In the area of precision medicine, an improved characterization of the primary tumor could help to plan a more personalized treatment strategy. In this perspective, the identification of imaging features associated with tumor-specific biologic properties and metastatic potential could be clinically relevant in women with VSCC. Some ^{18}F-FDG PET–related radiomics approaches have already been recently explored in other gynecologic malignancies such as cervical cancer (*15*).

The aim of this study was to investigate whether quantitative imaging features derived from ^{18}F-FDG PET/CT scans can be used to predict both biologic behavior of the vulvar malignancy and patient prognosis. An innovative method for identifying imaging features in the dataset was achieved by principal-component analysis (PCA) (*16*), an unsupervised technique to perform dimensionality reduction.

MATERIALS AND METHODS

Patients and Study Design

This retrospective study was approved by the Ethical Committee of the Fondazione Policlinico Universitario A. Gemelli-IRCCS (study code 1633). The medical records of all patients with histologically proven VSCC, referred to the Division of Gynecologic Oncology between June 2013 and December 2016, were reviewed. With their written informed consent, women were included if they were at least 18 y old, had a unifocal VSCC with stromal invasion more than 1 mm deep and diameter of at least 26 mm (*17*), underwent a preoperative ^{18}F-FDG PET/CT scan, received vulvar cancer surgery, and had at least 6 mo of follow-up data available. Women were excluded if they had multifocal vulvar cancer, a contraindication for surgery due to age or comorbidities, prior chemotherapy or locoregional radiation therapy within the last 5 y, prior locoregional surgery, or a plasma glucose level higher than 200 mg/dL before ^{18}F-FDG PET/CT acquisition. Surgical procedures and adjuvant treatments (radiotherapy with or without concomitant chemotherapy) were provided according to international guidelines after multidisciplinary decision making. Follow-up was performed every 3 mo for the first 2 y and every 6 mo up to the fifth year.

^{18}F-FDG PET/CT Image Acquisition

PET/CT studies were performed as previously described (*18*). Briefly, each patient fasted for at least 6 h. Following intravenous administration of 201 ± 58 MBq of ^{18}F-FDG, PET images were acquired after 66 ± 16 min using either a Gemini GXL (Philips Healthcare) or a Biograph mCT (Siemens Heathineers) PET/CT scanner. A low-dose CT scan (110–120 kVp, 20–40 mAs) was acquired for anatomic reference and attenuation correction purposes, followed by a PET scan using 2.5 min (Biograph) or 3 min (Gemini) per bed position. All PET images were reconstructed according to the European Association of Nuclear Medicine guidelines for tumor PET imaging (*19*) using either a line-of-response row-action maximum-likelihood algorithm (3 iterations and 33 subsets, voxel size of $4 \times 4 \times 4$ mm, no additional gaussian smoothing) or a 3-dimensional (3D) ordered-subsets expectation-maximization algorithm with resolution modeling (2 iterations and 21 subsets, voxel size of $3.2 \times 3.2 \times 5$ mm, additional gaussian smoothing of 8.2 mm in full width at half maximum) for the Gemini or Biograph, respectively.

Image Analysis

Radiomic analysis was performed on all ^{18}F-FDG PET/CT images using software built in-house (*20*), extracting 83 features based on intensity ($n = 23$), local intensity ($n = 1$), intensity-volume histograms ($n = 1$), morphology ($n = 14$), fractal ($n = 3$), or texture ($n = 41$) (Supplemental Table 1; supplemental materials are available at http://jnm.snmjournals.org). These features were derived from gray-level cooccurrence matrices or from gray-level run-length matrices that were calculated by merging the obtained matrices over all 13 directions while applying discretization with a fixed bin size of 0.25 g/mL (*20*). Only uniformity, entropy, and local entropy were also calculated, with discretization with 64 gray-level bins (*17,21*). All features were implemented according to the definitions set by the image biomarker standardization initiative (*22*).

All ^{18}F-FDG PET/CT images were reviewed by consensus between 2 experienced nuclear medicine physicians, masked to clinical and histopathologic information. Volumes of interest of the primary tumor were drawn semiautomatically on all PET images using an isocontour method that applied a 50% threshold of the SUV_{peak} corrected for local background activity (*23*). SUV_{peak} was defined as the highest SUV_{mean}

TABLE 1
Characteristics of the 40 Patients

Characteristic	Data
Mean age ± SD (y)	70 ± 10
Mean body mass index (kg/m^2)	27 (range, 16–42)
Mean time ± SD between PET/CT and surgery (d)	20 ± 17 (range, 1–74)
Primary vulvar tumor site	
Anterior	20 (50)
Lateral	17 (42.5)
Posterior	3 (7.5)
Tumor growth pattern	
Exophytic	29 (72.5)
Ulcerative	7 (17.5)
Infiltrative	4 (10)
Neighboring tissues involved	
Extravulvar skin	4 (10)
Urologic tract	4 (10)
None	32 (80)
Vulvar surgery	
Partial vulvectomy	6 (15)
Radical vulvectomy	34 (85)
Inguinofemoral lymph node surgery	
Unilateral	0
Bilateral	39 (97.5)
None	1 (2.5)
SLNB	3 (8)
SLNB followed by IFL	16 (41)
ILF	20 (51)
Pelvic lymph node surgery	
Unilateral	8 (20)
Bilateral	1 (2.5)
None	31 (77.5)

SLNB = sentinel lymph node biopsy; IFL 5 inguinofemoral lymphadenectomy.

Data are *n* followed by percentage in parentheses, unless otherwise specified.

TABLE 2
Histopatologic Characteristics, Staging, and Postoperative Therapy of the 40 Patients

Characteristic	Data
Tumor diameter (mm)	
Median	50 (range, 30–90)
26–40	17 (42.5)
>40	23 (57.5)
Histologic grade	
G1	2 (5)
G2	32 (80)
G3	6 (15)
Depth of stromal invasion (mm)	
Median	9 (range, 4–20)
1–4	3
>5	34
Unknown	3
Resection margin status	
R0	32 (80)
R1	4 (10)
VIN	4 (10)
Lymph-vascular space invasion	
Yes	19 (47.5)
No	21 (52.5)
Metastatic lymph nodes	
Yes	23 (57.5)
No	17 (42.5)
Extracapsular invasion of metastatic lymph nodes	
Yes	12 (52)
No	11 (48)
Median no. of removed lymph nodes	17 (range, 0–28)
Median no. of metastatic lymph nodes	1 (range, 0–7)
Median size of lymph node metastases (mm)	13 (range, 1–27)
FIGO stage	
IB	5 (12.5)
II	12 (30)
III	18 (45)
IVA	5 (12.5)
Adjuvant therapy	
Yes	27 (67.5)
No	13 (32.5)

G1 = well differentiated; G2 = moderately differentiated; G3 = poorly differentiated; R0 = no tumor; R1 = microscopic tumor; VIN = vulvar intraepithelial neoplasia; FIGO = International Federation of Gynecology and Obstetrics.

Data are *n* followed by percentage in parentheses, unless otherwise specified.

of a 1-mL sphere within the volume of interest, not necessarily centered around the SUV_{max} within the volume of interest. In cases of urinary contamination or the presence of high-uptake areas near the tumor (e.g., bladder), a freehand box was drawn that excluded the urinary contamination or other high-uptake areas before semiautomatic delineation.

Statistical Analysis

Dimensionality Reduction and Feature Selection. Radiomic features that correlated strongly ($r > 0.9$) were grouped, and only one feature from each group was selected as input for PCA. The dimensionality of radiomic features was then reduced by PCA (SPSS, version 23; IBM Statistics). During this analysis, an orthogonal rotation (varimax with Kaiser normalization) was applied to convert the set of linearly uncorrelated variables, also known as principal components, in such a way that the first principal component explained the largest possible variance in the dataset and each succeeding component had the highest variance possible under the constraint that it was orthogonal to the preceding components. To minimize false discoveries, no more than 4 principal components were allowed in the final analysis, since the rule of thumb is that at least 10 patients are required to test one radiomic feature (*24*). The sampling adequacy for each component in the model and for the complete model was determined by the Kaiser-Meyer-Olkin measure, which had to be 0.5 or higher.

Correlation of Radiomic Features with Histopathology. Radiomic features identified with PCA were correlated with histopathologic features such as histologic grade, depth of stromal invasion, presence of lymph-vascular space invasion, and metastatic lymph nodes. These features were tested for normality using the Shapiro–Wilk test. The significance of differences between histologic groups (grade, presence of lymph-vascular space invasion, and metastatic lymph nodes) was analyzed using the Mann–Whitney *U* test. Furthermore, linear regression was used to correlate the depth of stromal invasion with the radiomic features.

Correlation of Clinical Characteristics, Histopathologic Parameters, and Radiomic Features with Clinical Outcome. The correlation of clinical characteristics, histopathologic parameters, and radiomic features

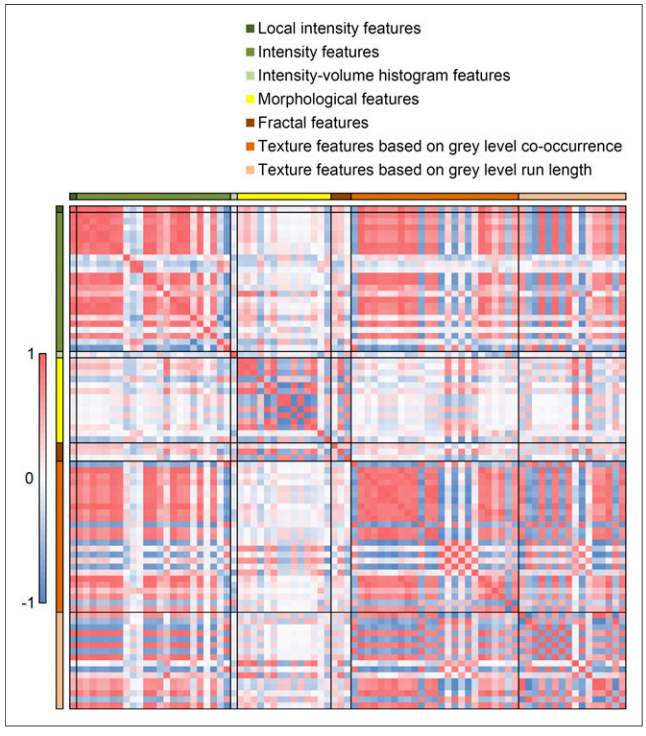

FIGURE 1. Correlation map for all radiomic features. Red = high positive correlation; blue = high negative correlation; white = no correlation.

TABLE 3
Follow-Up Closeout Data (February 2018)

Parameter	Data
Follow-up for entire study (mo)	
Median	15 (range, 2–50)
Mean ± SD	19 ± 13
Follow-up for surviving patients (mo)	
Median	26 (range, 6–50)
Mean ± SD	25 ± 13
PFS	
Median	10 (range, 2–50)
Mean ± SD	17 ± 14
OS	
Median	16 (range, 3–50)
Mean ± SD	20 ± 13
Local or distant recurrence (*n*)	18 (45%)*
Death (*n*)	18 (45%)†

*15 of these 18 patients died due to cancer progression.
†During median follow-up of 11 mo (mean, 12 ± 8; range, 2–34).

with prognosis was determined using univariate Cox regression analysis for progression-free survival (PFS) and OS. PFS was defined as the interval between surgery and the first clinical detection of recurrence. OS was defined as the interval between surgery and death. From the univariate Cox regression analysis, candidate covariates were identified for multivariate Cox regression models on the basis of significance level ($P \leq 0.2$). Multivariate Cox regression analyses were performed by an iterative forward and backward selection of the candidate covariates based on the likelihood ratio. Furthermore, survival curves were estimated using the Kaplan–Meier analysis. Variables were stratified in a low group and a high group at their median. The Kaplan–Meier curves were compared using the Mantel–Cox statistics. *P* values of less than 0.05 were considered statistically significant.

RESULTS

Patients

The records of 120 women with VSCC were reviewed. The inclusion criteria were fulfilled by 40 women, whose characteristics are summarized in Tables 1–3.

Data Dimensionality Reduction and Radiomic Feature Selection

Analysis of the 83 radiomic features revealed 19 prominent groups of strongly correlating features (Fig. 1; Supplemental Table 2), of which one feature per group was selected for PCA. Three of the 19 features (coefficient of variation, mean Laplacian, and kurtosis) did not meet the minimum Kaiser-Meyer-Olkin value of 0.5 and were excluded from the final model. The Kaiser-Meyer-Olkin value of the final model was middling (0.7). Four principal components were found that explained 84% of the variance, corresponding best to 4 radiomic features: SUV_{max}, local entropy (64 gray-level bins), maximum 3D diameter, and Moran's I (Supplemental Table 3). Moran's I did not show the best correlation with the component but showed the least correspondence to other components and was therefore selected instead of the area under the cumulative SUV–volume histogram curve (*25*).

Correlation of Radiomic Features with Histopathology

In 5 of 40 women, urinary contamination or high-uptake areas near the tumors were found and the delineation was adapted as mentioned earlier. No significant association was found between radiomic features and histologic grade (Table 4). Moreover, there was no strong correlation between depth of stromal invasion and radiomic features, as revealed by linear regression. Furthermore, radiomic features of the primary tumor were not predictive for presence of lymph-vascular space invasion or metastatic lymph nodes.

Correlation of Clinical and Histopathologic Characteristics with Clinical Outcome

As shown in Table 5, univariate Cox regression analysis revealed that, in this patient cohort, age was not predictive for PFS ($P = 0.06$) but was significantly associated with OS ($P = 0.006$). Regarding the histopathologic features from the primary tumor, lymph-vascular space invasion was not significantly associated with PFS ($P = 0.08$) but was significantly associated with OS ($P = 0.03$). Furthermore, number of metastatic lymph nodes, bilateral inguinofemoral lymph node metastases, and extracapsular invasion of metastatic lymph nodes were significantly associated with both PFS and OS.

Correlation of Radiomic Features with Clinical Outcome

None of the 4 radiomic features were statistically significantly associated with PFS. Only Moran's I correlated with OS ($P = 0.03$; Table 5). During multivariate Cox regression analysis, extracapsular invasion of the metastatic lymph node and Moran's I were found to be independent prognostic factors for PFS and OS (Table 5).

TABLE 4
Association Between Histopathologic Characteristics and Imaging Features Derived from ^{18}F-FDG PET Images

Radiomic feature	Histologic grade			Depth of invasion (mm)	Lymph-vascular space invasion			Metastatic lymph nodes		
	1–2	3	*P*		No	Yes	*P*	No	Yes	*P*
SUV_{max}	12.1 ± 4.2	13.9 ± 3.0	0.3	$R^2 = 0.07$	11.2 ± 3.2	13.7 ± 4.48	0.05	11.5 ± 4.2	13.0 ± 3.9	0.2
Local entropy	3.9 ± 0.11	3.9 ± 0.09	1	$R^2 = 0.10$	3.9 ± 0.12	3.9 ± 0.10	0.6	3.9 ± 0.10	3.9 ± 0.11	0.4
Maximum 3D diameter	48.5 ± 19.4	44.6 ± 16.1	0.8	$R^2 = 0.08$	47.6 ± 22.0	48.3 ± 15.0	0.7	46.9 ± 20.2	48.6 ± 18.0	0.9
Moran's I	0.062 ± 0.018	0.057 ± 0.021	0.8	$R^2 = 0.013$	0.059 ± 0.018	0.064 ± 0.020	0.6	0.062 ± 0.017	0.061 ± 0.020	0.9

R^2 indicates the coefficient of determination.

TABLE 5
Univariate and Multivariate Cox Regression Analysis for PFS and OS

Parameter	PFS		OS	
	Hazard ratio	*P*	Hazard ratio	*P*
Univariate Cox regression analysis				
Age	1.1 (1.0–1.1)	0.06	1.1 (1.0–1.1)	0.006
Maximum diameter of primary tumor	1.0 (0.8–1.4)	0.9	1.1 (1.0–1.1)	0.6
Histologic grade		0.8		0.3
I–II	1		1	
III	0.9 (0.3–3.0)		0.6 (0.2–1.7)	
Lymph-vascular space invasion	2.3 (0.9–6.1)	0.08	3.0 (1.1–7.9)	0.03
Depth of stromal invasion	1.0 (0.9–1.2)	0.4	1.1 (0.9–1.2)	0.4
Resection margin status		0.6		0.4
R0	1		1	
R1	2.5 (0.3–18.7)		3.3 (0.4–25.3)	
VIN	1.9 (0.2–21.4)		2.5 (0.2–27.4)	
Metastatic lymph nodes*	2.1 (0.7–5.9)	0.2	3.0 (1.0–9.2)	0.05
Bilateral metastatic lymph nodes	3.0 (1.2–7.6)	0.02	2.7 (1.0–6.8)	0.04
Number of metastatic lymph nodes*	1.3 (1.0–1.5)	0.02	1.3 (1.0–1.5)	0.03
Extracapsular invasion of metastatic lymph nodes	5.3 (2.1–13.7)	<0.0001	4.2 (1.6–10.6)	0.003
FIGO stage		0.4		0.1
IB	1		1	
II	0.6 (0.1–3.9)		0.7 (0.01–5.0)	
III	0.3 (0.06–1.5)		0.4 (0.05–2.6)	
IVA	0.8 (0.2–3.0)		1.7 (0.4–7.6)	
Radiomic feature				
SUV_{max}	1.0 (0.9–1.2)	0.6	1.0 (0.9–1.1)	0.6
Local entropy	1.7 (0.03–99.1)	0.8	0.6 (0–33.2)	0.8
3D maximum diameter	1.0 (1.0–1.0)	0.5	1.0 (1.0–1.0)	0.8
Moran's I	1.3 (1.0–1.6)	0.06	1.3 (1.0–1.7)	0.03
Multivariate Cox regression analysis				
Iterative forward selection				
Extracapsular invasion	9.5 (3.1–28.6)	<0.0001	6.5 (2.3–18.4)	<0.0001
Moran's I	1.6 (1.2–2.3)	0.03	1.5 (1.1–2.1)	0.009
Iterative backward selection				
Extracapsular invasion	9.5 (3.1–28.6)	0.0001	4.3 (1.4–12.6)	0.009
Moran's I	1.6 (1.2–2.3)	0.03	1.4 (1.1–2.0)	0.02

*Metastatic lymph nodes indicates patients with metastatic lymph nodes; number of metastatic lymph nodes is the number of metastatic lymph nodes per patient.

R0 = no tumor; R1 = microscopic tumor; VIN = vulvar intraepithelial neoplasia; FIGO = International Federation of Gynecology and Obstetrics.

Data in parentheses are 95% confidence intervals.

Estimated Kaplan–Meier survival curves revealed that the PFS and OS curves of the 4 radiomic features did not significantly differ (Fig. 2). The PFS and OS curves of the low and high group of SUV_{max}, local entropy, and maximum 3D diameter showed high similarity and no clear separation (Fig. 2). For Moran's I, the survival curves showed a clear separation, albeit nonsignificant, between the low and high groups, particularly at later times (Fig. 2). A tendency associating a low value of Moran's I with a longer PFS and OS was observed. Figure 3 shows ^{18}F-FDG PET/CT images of 2 women with VSCC with either a high or a low Moran's I value.

DISCUSSION

This retrospective study evaluated the clinically added value of quantitative imaging features, also known as radiomic features,

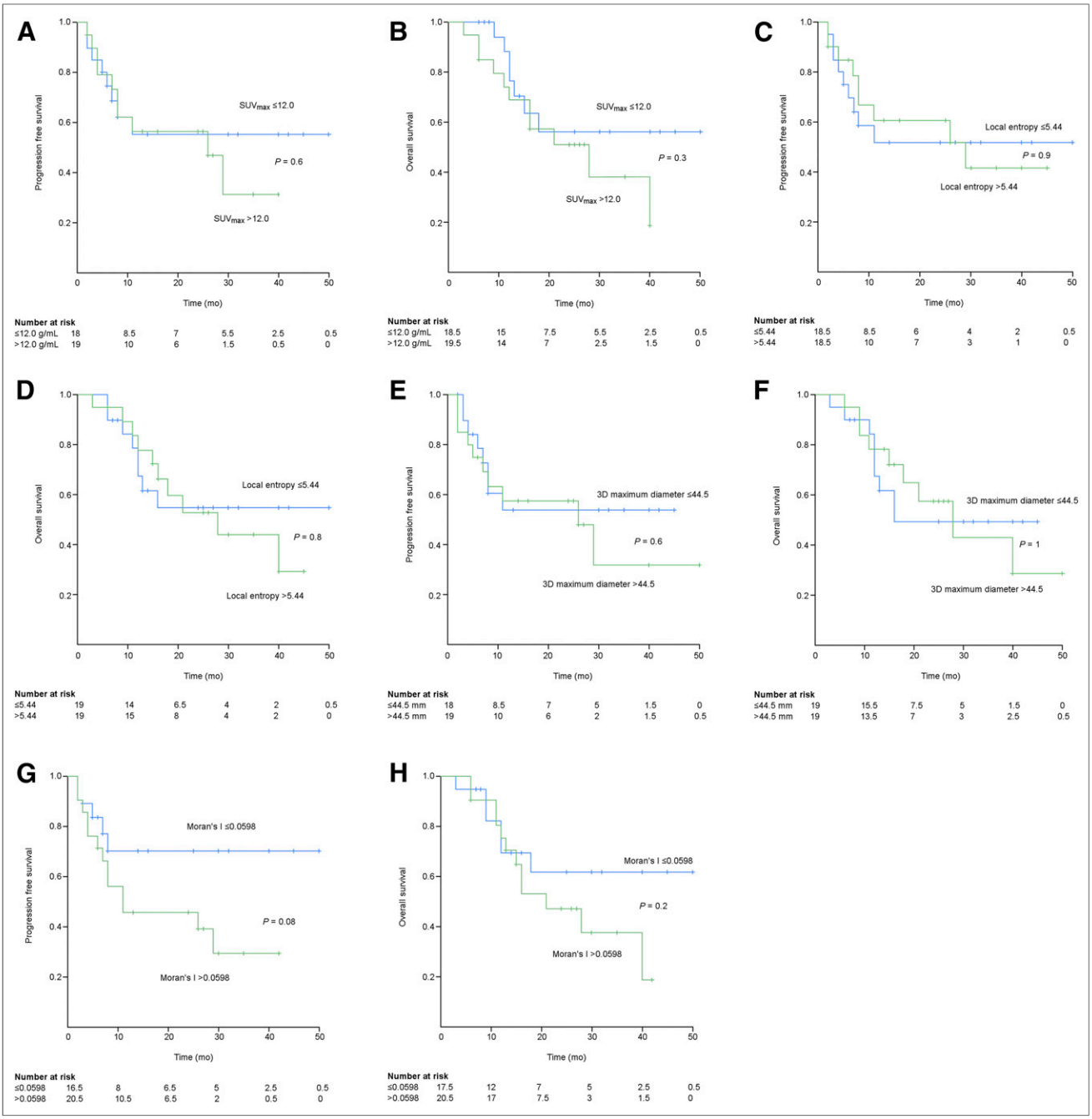

FIGURE 2. Estimated Kaplan–Meier curves for PFS of SUV_{max} (A), OS of SUV_{max} (B), PFS of local entropy (C), OS of local entropy (D), PFS of 3D maximum diameter (E), OS of 3D maximum diameter (F), PFS of Moran's I (G), and OS Moran's I (H).

derived from preoperative ^{18}F-FDG PET/CT images to predict both tumor biology and patient prognosis in VSCC. Especially, the identification of radiomic features able to predict aggressiveness and poor prognosis before treatment may be of great value for planning a more personalized treatment strategy (e.g., surgery) in women with VSCC.

To the best of our knowledge, no prior studies have evaluated radiomics in vulvar cancer or used PCA to select unique radiomic features from a dataset with a limited number of patients. In radiomics studies, the problem of multiple testing, or the look-elsewhere effect, yields the problem of finding falsely statistically significant results (*14,16,24*). We addressed this problem by performing dimensionality reduction, leaving only 4 imaging features that explained most of the variance of our dataset.

On the basis of our findings, the identified image features correlated poorly with histopathologic features. A possible explanation may be that we included only women whose primary tumor was at least 26 mm in diameter. In accordance with previous publications, this minimum size was chosen to reliably quantify tracer uptake heterogeneity features (*17*), but hereby, the considered patient cohort may lack variation. Furthermore, only 6 women were diagnosed with a histologic grade 3 tumor, and the depth of stromal invasion

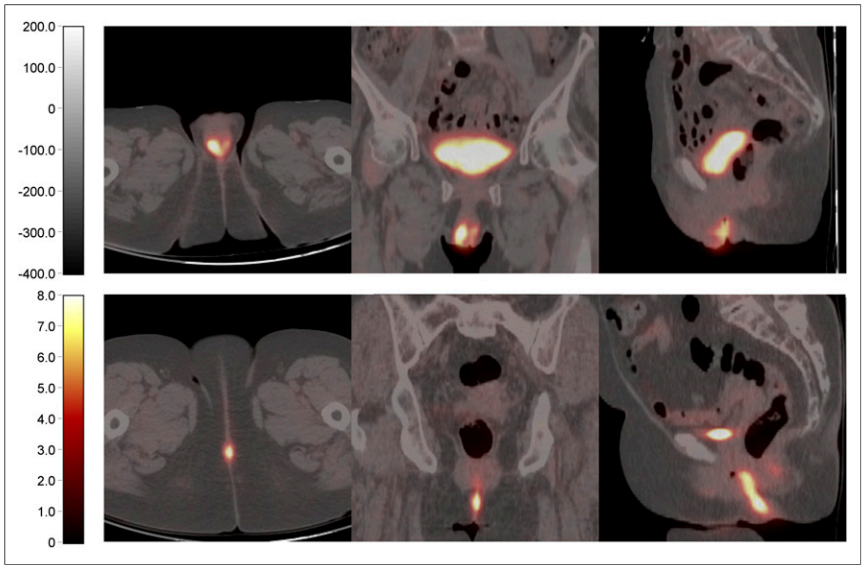

FIGURE 3. From left to right, transverse, coronal, and sagittal ^{18}F-FDG PET/CT images of 2 women with vulvar carcinoma. (Top) An 81-y-old woman who had anterior midline 4-cm-diamter tumor with heterogeneous ^{18}F-FDG uptake and relatively high Moran's I (0.0924). Inguinal lymph node recurrence and death occurred 4 and 16 mo after surgery, respectively. (Bottom) A 74-y-old woman who had posterior midline 3-cm-diamter tumor with homogeneous ^{18}F-FDG uptake and low Moan I (0.0213). At time of last follow-up, patient was alive and without recurrence.

was principally more than 4 mm, limiting the possibility of investigating the correlation between radiomic and these histopathologic features.

In our study, parameters such as age, lymph-vascular space invasion, and lymph node features were prognostic factors for PFS or OS. This finding is concordant with the literature and emphasizes that these parameters are risk factors for the prognosis of patients with vulvar cancer (*8*). In contrast, none of the selected radiomic features were found to be a prognostic factor for PFS at univariate analysis, although Moran's I almost reached significance. Nevertheless, Moran's I found a prognostic factor for OS at univariate analysis and an independent prognostic factor for PFS and OS at multivariate analysis. In detail, Moran's I is a radiomic feature that reflects the global spatial autocorrelation of the voxels, and its value ranges from −1 to 1, where −1 reflects a perfect dispersion of the voxels, 0 reflects a completely random placement, and 1 reflects a perfect clustering (*22*). Our results showed that a higher Moran's I value, reflecting a higher degree of clustering voxels with similar uptake (i.e., an indication of tracer uptake heterogeneity), predicts a high risk of recurrence and poor survival. On the basis of our results, Moran's I appears to be usable in predicting the prognosis before treatment. Thus, if confirmed by further, larger, studies, Moran's I could be included in the parameters considered in treatment planning.

Although both the PFS and the OS Kaplan–Meier curves of the low and high group of Moran's I showed no significant difference, a tendency associating Moran's I low values with longer PFS and OS was observed. One likely explanation for nonsignificance may be the relatively short median follow-up for some patients. However, only 4 living patients had a follow-up of less than 12 mo.

The relatively small sample size, which reflects the low incidence of vulvar cancer (*1,2*), may be another reason for the borderline association. Another possible underlying cause could be the middling PCA results, with a Kaiser-Meyer-Olkin value of 0.7. Although this value is higher than the minimal requirement (Kaiser-Meyer-Olkin $>$ 0.5), the value should ideally be higher to make definitive conclusions. A larger number of patients are needed to have a more reliable PCA. Therefore, we recommend that a large multicenter study be designed to validate the results obtained from this study. To facilitate multicenter studies, future studies should focus on further standardization of image acquisition methods, reconstruction settings, segmentation methods (*14,19*), and radiomic analysis (*22*).

In this study, the clinically added value of ^{18}F-FDG PET as a single imaging modality was investigated. However, combination of information derived from different imaging modalities, including MRI and CT, may complement the information concerning tumor biology. This possibility was recently emphasized in a study involving patients with locally advanced cervical cancer (*26*). In that study, combined radiomic analysis of both ^{18}F-FDG PET and diffusion-weighted MRI was able to predict patient outcome after chemoradiotherapy.

There were several limitations to our study. First, it was a retrospective, single-center study. Second, it concerned a relatively small patient cohort with a low incidence of gynecologic malignancy (*1,2*). Third, a bias concerning population selection was introduced; however, this bias is required for radiomics (*17*). Finally, our results should be interpreted with caution because of the relatively short median follow-up.

CONCLUSION

The present study showed that PCA may be used to perform dimensionality reduction for radiomics, going beyond commonly used radiomic features in the current clinical workup, such as SUV_{max} or maximum diameter. Although the identified features poorly predicted the biologic characteristics of the primary tumor, Moran's I was identified as an independent prognostic predictor for PFS and OS. However, the explorative character of this study demands further validation in larger, prospective multicenter studies.

DISCLOSURE

No potential conflict of interest relevant to this article was reported.

ACKNOWLEDGMENTS

We thank Emiliano Barbante for his help in the collection of PET data and Marianne Valdés Olmos for language editing.

REFERENCES

1. Howlader N, Noone AM, Krapcho M, et al. SEER cancer statistics review, 1975–2013. National Cancer Institute website. http://seer.cancer.gov/csr/1975_2013/. Updated September 12, 2016. Accessed September 27, 2018.
2. Bayne L, Butler J, Colombo N, et al. Gynaecological cancers in Europe: facts and figures 2015. ASACO website. http://www.asociacionasaco.es/wp-content/uploads/2015/10/Facts-datos-y-figures-estadisticas-2015-imprimible.pdf. Published September 2015. Accessed September 27, 2018.

3. Eifel PJ, Berek JS, Markman MA. Cancer of the cervix, vagina, and vulva. In: DeVita VT Jr, Lawrence TS, Rosenberg SA, eds. *Cancer: Principles and Practice of Oncology.* 9th ed. Philadelphia, PA: Lippincott Williams and Wilkins; 2011: 1311–1344.
4. Del Pino M, Rodriguez-Carunchio L, Ordi J. Pathways of vulvar intraepithelial neoplasia and squamous cell carcinoma. *Histopathology.* 2013;62(suppl 1):161–175.
5. Hacker NF. Vulvar cancer. In: Berek JS, Hacker NF, eds. *Practical Gynecologic Oncology.* 4th ed. Philadelphia, PA: Williams and Wilkins; 2005:585–602.
6. Homesley HD, Bundy BN, Sedlis A, et al. Assessment of current International Federation of Gynecology and Obstetrics staging of vulvar carcinoma relative to prognostic factors for survival (a Gynecologic Oncology Group study). *Am J Obstet Gynecol.* 1991;164(suppl 4):997–1003.
7. Burger MP, Hollema H, Emanuels AG, Krans M, Pras E, Bouma J. The importance of the groin node status for the survival of T1 and T2 vulval carcinoma patients. *Gynecol Oncol.* 1995;57(suppl 3):327–334.
8. Koh WJ, Abu-Rustum NR, Bean S, et al. NCCN Clinical Practice Guidelines in Oncology (NCCN guidelines), Vulvar cancer (squamous cell carcinoma): version 1.2019. https://www.nccn.org/professionals/physician_gls/pdf/vulvar.pdf. Updated August 30, 2018. Accessed September 27, 2018.
9. Levenback CF, Ali S, Coleman RL, et al. Lymphatic mapping and sentinel lymph node biopsy in women with squamous cell carcinoma of the vulva: a gynecologic oncology group study. *J Clin Oncol.* 2012;30(suppl 31):3786–3791.
10. Van der Zee AG, Oonk MH, De Hullu JA, et al. Sentinel node dissection is safe in the treatment of early-stage vulvar cancer. *J Clin Oncol.* 2008;26(suppl 6): 884–889.
11. Garganese G, Collarino A, Fragomeni SM, et al. Groin sentinel node biopsy and ^{18}F-FDG PET/CT-supported preoperative lymph node assessment in cN0 patients with vulvar cancer currently unfit for minimally invasive inguinal surgery: the GroSNaPET study. *Eur J Surg Oncol.* 2017;43(suppl 9):1776–1783.
12. Oonk MHM, Planchamp F, Baldwin P, et al. European Society of Gynaecological Oncology guidelines for the management of patients with vulvar cancer. *Int J Gynecol Cancer.* 2017;27(suppl 4):832–837.
13. Lambin P, Rios-Velazquez E, Leijenaar R, et al. Radiomics: extracting more information from medical images using advanced feature analysis. *Eur J Cancer.* 2012;48(suppl 4):441–446.
14. Hatt M, Tixier F, Pierce L, Kinahan PE, Le Rest CC, Visvikis D. Characterization of PET/CT images using texture analysis: the past, the present. . . any future? *Eur J Nucl Med Mol Imaging.* 2017;44(suppl 1):151–165.
15. Tsujikawa T, Rahman T, Yamamoto M, et al. ^{18}F-FDG PET radiomics approaches: comparing and clustering features in cervical cancer. *Ann Nucl Med.* 2017;31(suppl 9):678–685.
16. Limkin EJ, Sun R, Dercle L, et al. Promises and challenges for the implementation of computational medical imaging (radiomics) in oncology. *Ann Oncol.* 2017;28(suppl 6):1191–1206.
17. Hatt M, Majdoub M, Vallières M, et al. ^{18}F-FDG PET uptake characterization through texture analysis: investigating the complementary nature of heterogeneity and functional tumor volume in a multi-cancer site patient cohort. *J Nucl Med.* 2015;56(suppl 1):38–44.
18. Collarino A, Garganese G, Valdés Olmos RA, et al. Evaluation of dual-timepoint ^{18}F-FDG PET/CT imaging for lymph node staging in vulvar cancer. *J Nucl Med.* 2017;58(suppl 12):1913–1918.
19. Boellaard R, Delgado-Bolton R, Oyen WJ, et al. FDG PET/CT: EANM procedure guidelines for tumour imaging: version 2.0. *Eur J Nucl Med Mol Imaging.* 2015;42(suppl 2):328–354.
20. van Velden FH, Kramer GM, Frings V, et al. Repeatability of radiomic features in non-small-cell lung cancer [^{18}F]FDG-PET/CT studies: impact of reconstruction and delineation. *Mol Imaging Biol.* 2016;18(suppl 5):788–795.
21. Tixier F, Hatt M, Le Rest CC, Le Pogam A, Corcos L, Visvikis D. Reproducibility of tumor uptake heterogeneity characterization through textural feature analysis in ^{18}F-FDG PET. *J Nucl Med.* 2012;53(suppl 5):693–700.
22. Zwanenburg A, Leger S, Vallières M, Löck S. Image biomarker standardisation initiative. https://arxiv.org/abs/1612.07003. arXiv.org website. Updated September 17, 2018. Accessed September 27, 2018.
23. Frings V, van Velden FH, Velasquez LM, et al. Repeatability of metabolically active tumor volume measurements with FDG PET/CT in advanced gastrointestinal malignancies: a multicenter study. *Radiology.* 2014;273(suppl 2):539–548.
24. Chalkidou A, O'Doherty MJ, Marsden PK. False discovery rates in PET and CT studies with texture features: a systematic review. *PLoS One.* 2015;10(suppl 5): e0124165.
25. van Velden FH, Cheebsumon P, Yaqub M, et al. Evaluation of a cumulative SUV-volume histogram method for parameterizing heterogeneous intratumoural FDG uptake in non-small cell lung cancer PET studies. *Eur J Nucl Med Mol Imaging.* 2011;38(suppl 9):1636–1647.
26. Lucia F, Visvikis D, Desseroit MC, et al. Prediction of outcome using pretreatment ^{18}F-FDG PET/CT and MRI radiomics in locally advanced cervical cancer treated with chemoradiotherapy. *Eur J Nucl Med Mol Imaging.* 2018;45(suppl 5): 768–786.